Available online at www.sciencedirect.com
SCIENCE DIRECT®
Journal of Electroanalytical Chemistry 566 (2004) 341–350
Journal of Electroanalytical Chemistry
www.elsevier.com/locate/jelechem

The influence of sodium diphenylamine sulfonate on the electrodeposition of Mg–Ni alloy and its electrochemical characteristics

Longbiao Liao [a,*], Weihong Liu [b], Xianming Xiao [a]

[a] State key Laboratory of Organic Geochemistry, Guangzhou Institute of Geochemistry, Chinese Academy of Sciences, Guangzhou 510640, PR China
[b] Department of Chemistry, New Campus, Shanghai University, Shanghai 200436, PR China

Received 28 August 2003; received in revised form 1 October 2003; accepted 18 November 2003

Abstract

Voltammetric measurements showed that sodium diphenylamine sulfonate (SDS) could inhibit hydrogen evolution and form complexes with nickel and magnesium ions for Mg–Ni alloy electrodeposition. The characteristics of differential capacity curves from differential pulse anodic stripping voltammetry showed that SDS had an absorption effect on the cathode electrode. Steady state cathode polarization of Mg–Ni alloy measurements on rotating disk copper electrodes were performed, the relative results from the polarization curves indicated that SDS acted as a levelling agent. The phases and morphology of Mg–Ni alloy were examined by X-ray diffraction and scanning electron microscopy. A series of spectra showed that phenothiazine codeposited with Mg–Ni alloy. The value 0.9 of H/M (M = Mg–Ni alloy) was determined by pressure–composition isotherm measurements. The maximum discharge capacity of the alloy was 388 mA h/g; the decay of discharge capacity was studied by electrochemical impedance spectroscopy measurements.

Keywords: Sodium diphenylamine sulfonate; Levelling agent; Phenothiazine

1. Introduction

Mg–Ni alloy, famous for its good hydrogen absorption and low cost, has been regarded as one of the most promising hydrogen storage materials. Many groups prepared Mg–Ni alloy by mechanical alloying [1–3]. We first obtained Mg–Ni alloy film by electrodeposition from an aqueous system, in which many organic additives might play a role. The mechanisms of additives in electroplating processes from an aqueous system are fairly complex. Part of the difficulty in understanding the effects of additives is the fact that all electrodeposition processes involve a competition between at least two procedures: the reduction or crystallization of the metal or alloy and the reduction of the solvent [4]. To date, many models in these studies have been proposed, such as: one could increase the current efficiency for processes either by inhibiting the electrolysis of water or by catalyzing the desired electrochemical processes [4], one could inhibit the oxidation of water by the formation of hydrophobic films [5], one could decrease the reduction potential of the metal [6], one could inhibit the reduction of water by the formation of insoluble films of inorganic compounds [7], or one could increase the limiting reduction current [8]. Franklin and coworkers found that organic compounds were absorbed on the metal surfaces by inhibiting the rates of the redox reaction [9], changing the concentration of redox reaction species [10], shifting equilibrium potentials at the electrode [10]. Therefore, SDS appeared to be an interesting organic additive. This study aims to explain the effect of SDS on Mg–Ni alloy film deposition, and on this basis, we also explained the electrochemical behavior of Mg–Ni alloy film.

* Corresponding author. Tel./fax: +86-020-85290176.
E-mail addresses: lbliao@gig.ac.cn, liaolb@sina.com.cn (L. Liao).

0022-0728/$ - see front matter © 2003 Published by Elsevier B.V.
doi:10.1016/j.jelechem.2003.11.045

2. Experimental

The composition of the plating bath was similar to that in the previous study, namely, 0.4 $g\,ml^{-3}MgCl_2 \cdot 6H_2O$ + $MgSO_4 \cdot 6H_2O$ or 0.1 $g\,ml^{-3}$ $NiCl_2 \cdot 6H_2O$ + $Ni_2SO_4 \cdot 6H_2O$, 0.025 $g\,ml^{-3}H_3BO_3$, 0.015 $g\,ml^{-3}$ SDS, and six other additives were used at 0.01 $g\,ml^{-3}$. The pH was 6.7, at a constant current density of 83 $mA\,cm^{-2}$, the solution was deaerated by N_2 bubbles before plating and the working and counter electrodes were made of commercial copper (99.85%). The bath without SDS was bath1, from which alloy1 was deposited, the bath with SDS was bath2, from which alloy2 was deposited.

Voltammetric measurement was used as the exploratory technique to determine the effect of the SDS on the rate of hydrogen evolution and Mg–Ni alloy deposition. The voltammetric studies were performed with Pt wire cathodes and anodes.

The rotating copper disk ($\Phi = 60$, ATA-1 A) experiments were performed by cathodic polarization measurements, the side-edge of the copper was wrapped tightly with Teflon tape. A Pt plate (1.1 cm^{-2}) was used as the counter electrode. All of the voltammetry, polarization and EIS measurements were carried out on a CHI660-A electroanalytical workstation with a PC, in which the reference electrode was a saturated calomel electrode (SCE), at room temperature. Differential pulse anodic stripping voltammetry (DPASV) measurement was performed on a plating analyzer (DD-1), for which the maximum area of the hanging mercury drop electrode (HMDE) was 1.12×10^{-2} cm^2. The cell testing was performed with a Land-cell test system, linked to the PC. The test cell was composed of three electrodes, the working electrode was the Mg–Ni alloy film electrode resulting from the deposition, the counter electrode was $Ni(OH)_2$ and the reference electrode was Hg|HgO|6 M KOH. The reference electrode was equipped with a Luggin tube to reduce the *IR* drop in the testing. The electrolyte was 6 M KOH aqueous solution and the temperature was held at 30 ± 1 °C. The alloy electrode was charged galvanostatically at 50 $mA\,g^{-1}$ for 9 h, and after resting for 5 min, it was discharged at 50 $mA\,g^{-1}$ until the potential reached −0.60 V vs. Hg|HgO|6 M KOH. EIS measurements were performed with scanning frequencies ranging from 10 kHz to 0.01 Hz and an ac amplitude of 5 mV at −0.75 V open-circuit voltage.

The phase and the composition of the Mg–Ni alloy was determined by powder XRD, with a D_8-Advance X-ray diffractometer using Cu Kα as the radiation source and a position sensitive detector for the identification of the different phases. The morphology was examined by scanning electron microscopy (SEM), which was carried out using an XL30 D6716 and was equipped with a Noran Vantage energy dispensive X-ray analyzer (EDX). The pressure–composition isotherm (PCT) measurements were performed at 313 K using a Sieverts-type apparatus, at 90 °C. Equilibrium was assumed to be established for each point when the pressure change $\Delta P/\Delta t$ reached 1×10^4 $atm\,h^{-1}$, when exposed to hydrogen gas under a constant pressure of 0.05 MPa. The number of hydrogen molecules reacting with the sample was calculated from the pressure drop during the hydriding process, and the value of H/M could be estimated. For an analysis of the existence of phenothiazine, the sample of Mg–Ni alloy was treated by inductively coupled plasma (ICP) [11], and then was examined by mass spectroscopy (MS) using a 4510-MS apparatus, infrared spectroscopy (IR) using a Nicolet 750-Fourier shift IR apparatus and a pressed plate with KBr and nuclear magnetic resonance (^{1}H NMR) using a JEOL 90GX.

3. Results and discussion

3.1. The influence of SDS on the electrodeposition of Mg–Ni alloy

3.1.1. Voltammetric responses

The voltammetric measurements were carried out in bath1 and bath2 and the voltammetric curves are shown in Fig. 1. The response of bath1 is curve a, the response of bath2 is curve b, Curve c is the response of bath2 + 0.005 $g\,ml^{-3}$ SDS. Curve a shows that alloy deposition began at −0.62 V, compared to curves a–c had the same normal deposition at about −0.62 V as the deposition in bath1. SDS caused: (1) a negative shift of the hydrogen evolution potential, (2) the formation of two current density waves for the alloy deposition, the first occurring at normal potential for alloy deposition as in bath1 and the second occurring at −0.79 V, (3) a decrease of

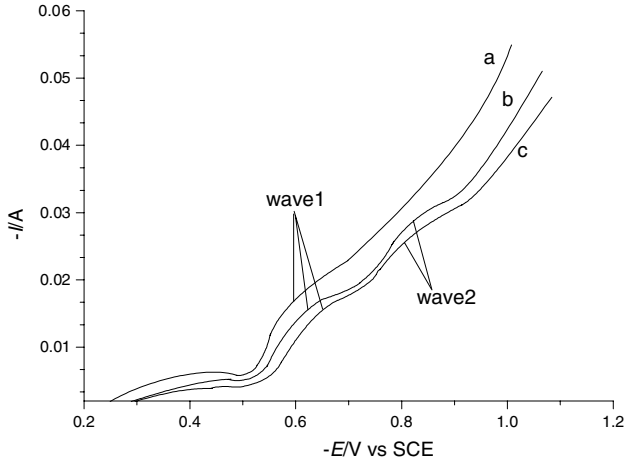

Fig. 1. The voltammetric responses of (a) bath1, (b) bath2 and bath2+0.005 $g\,ml^{-3}$ SDS.

the limiting current density of alloy deposition when the concentration of SDS was increased. Therefore, SDS blocked the hydrogen evolution by a negative shift of the hydrogen evolution potential and lowered the rate of alloy deposition. This could be explained qualitatively by assuming that: an organic compound was absorbed on the cathode electrode in bath2 (DPASV confirmed the absorption effect), because of its hydrophobic properties and its low dielectric constant. The cathode electrode became more hydrophobic and the dielectric constant in the neighborhood of the cathode electrode became lower than that of bath1. The former mechanically blocked the reduction of hydrogen, nickel and magnesium ions directly. The latter could cause an appreciable change in equilibrium and rate constant [5], or change the concentration of absorbed ions, cause a shift of the equilibrium potentials [6,7,10] and of the deposition potential [4]. The second current density wave, as shown in curves b and c, could be ascribed to the deposition of the SDS complex with nickel and magnesium ions. It was reported that SDS could complex with Ni^{2+}, Mg^{2+} [12] and comparing curves b with c, we found that SDS could lower the alloy deposition rate by a negative shift of the alloy deposition potential, and this could also be confirmed by EDX analysis. The result was in agreement with the character of saccharin in Ni–Fe–Cr alloy deposition studied by Harris and Whitely [13].

3.1.2. DPASV responses

DPASV measurements were carried out on the HMDE in bath1 and bath2. The responses are shown in Fig. 2. Curve a is the response of bath1, curve d is the response of bath2. There is an absorption peak in curve a, a saturated absorption peak begins to appear in curve d, and the differential capacity values becomes greater with a shift to negative potential. At −0.65 V, the two curves cross at P. Simultaneously, at −0.89, −1.25 and −1.31 V, curve d shows three capacity peaks. The peaks at −1.25 and −1.31 V showed greater capacity values than that at −0.89 V.

For the analysis of the three capacity peaks of curve d, three DPASV measurements were performed in bath2, which contained different concentrations of SDS. The responses of three of these are shown in Fig. 3. At −0.89 V, the capacity peak was wide and weak; according to Wang [14], this was an absorption peak, at −1.25 V, which showed the absorption effect of SDS. The peak potential shifted to more negative potential with increasing concentration. As in the theory of Trasatti [15], it was a desorption peak. At −1.31 V, the capacity value of the peak became greater with increasing concentration of SDS, but the potential of the peak did not change. From the conclusions of Reeves [16], this was the reduction peak of SDS. The reduction of SDS could be confirmed by a series of spectral measurements and pre-sputter analysis by EDX. Thus, SDS had an absorption effect on the electrode. The absorption of the additive on the electrode was studied by Yang and Zhou in the Ni–Zn deposition [17], in which the relative properties of DPASV were shown to be similar to those described above.

3.1.3. RDE polarization responses

Fig. 3 shows the cathode polarization curves at the RDE from 1000 to 2500 rpm for bath1 and bath2. At some fixed potentials, the current densities increased with an increase of the rotation rate of the electrode in bath1. The opposite changes occurred in bath2, and

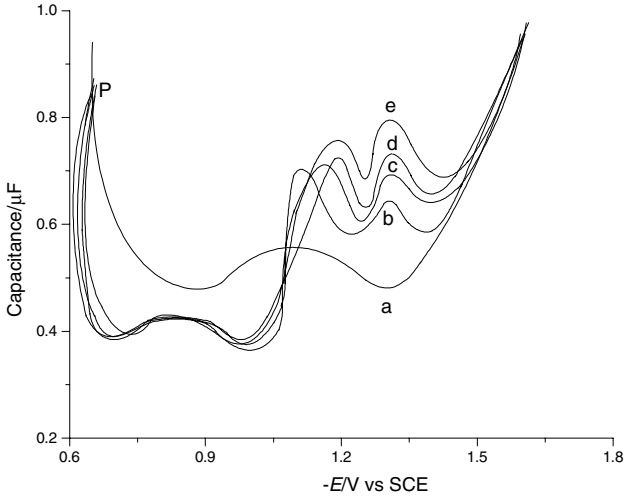

Fig. 2. The differential capacity curves for Hg electrodes: (a) bath1, (b) bath1+0.005 g ml^{-3} SDS, (c) bath1+0.01 g ml^{-3} SDS, (d) bath2 and (e) bath1+0.025 g ml^{-3} SDS, scan rate 5 mV s^{-1}.

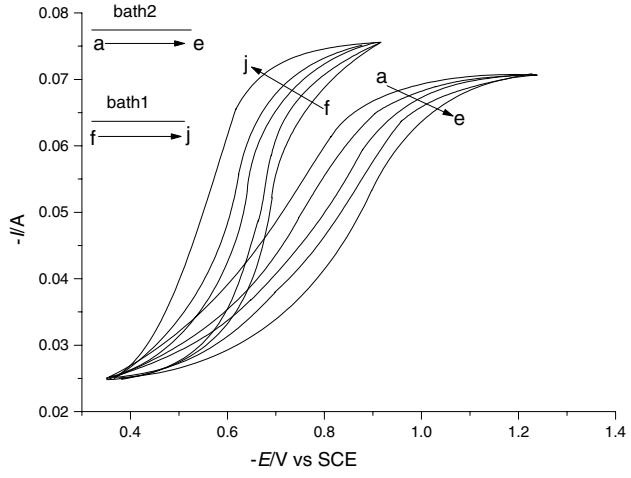

Fig. 3. Cathode polarization curves for the rotating disk electrodes, bath2: (a) 1000 rpm , (b) 1500 rpm, (c) 2000 rpm, (d) 2500 rpm and 3000 rpm, bath1: (f) 1000 rpm, (g) 1500 rpm, (h) 2000 rpm, (i) 2500 rpm (j) 3000 rpm.

both appeared to be limiting current densities, which suggested that the deposition on the RDE was under some sort of limiting control. A detailed analysis of the kinetics was not attempted here, since it was reasonable that for the Mg–Ni alloy deposited in the region between −0.5 and −0.9 V in bath1, and in the higher potential region from −0.6 to −1.1 V, the shift of the potential was in line with that for Fig. 1.

It is known that coumarin acts as a levelling agent in Ni plating [18–20]. Royers and Taylor [18], Kardos [19] and Kruylikly et al. [20] all studied the mechanism of coumarin, used as a levelling agent in the nickel plating process. These authors found that coumarin as a levelling agent showed two characteristics : (1) a linear dependence of the current I on the square root of the rotating speed $\omega^{1/2}$, (2) I decreased with the increase of $\omega^{1/2}$ at RDE.

As can be seen in Fig. 3, at −0.6 V, the deposition begins in both baths. At potentials more negative than −0.9 V, the hydrogen evolution dominates, so that the middle potential −0.8 V was studied. The corresponding $I-\omega^{1/2}$ values for bath1 and bath2 at −0.8 V are shown in Table 1. The plots from Table 1 are displayed as Fig. 4. For bath1, I increased with $\omega^{1/2}$, for bath2, the opposite was true. This showed not only an almost linear $I-\omega^{1/2}$ relationship but also I decreased with $\omega^{1/2}$, in accord with the report of Royers and Taylor [18].

Table 1
The relation of I vs. $\omega^{1/2}$ for bath1 and bath2

ω (rpm)	$\omega^{1/2}$ (rpm$^{1/2}$)	bath1($-I$/A)	bath2($-I$/A)
1000	31.62	0.0601	0.064
1500	38.73	0.0672	0.0571
2000	44.72	0.0716	0.054
2500	50	0.0735	0.0492
3000	55.77	0.0747	0.0447

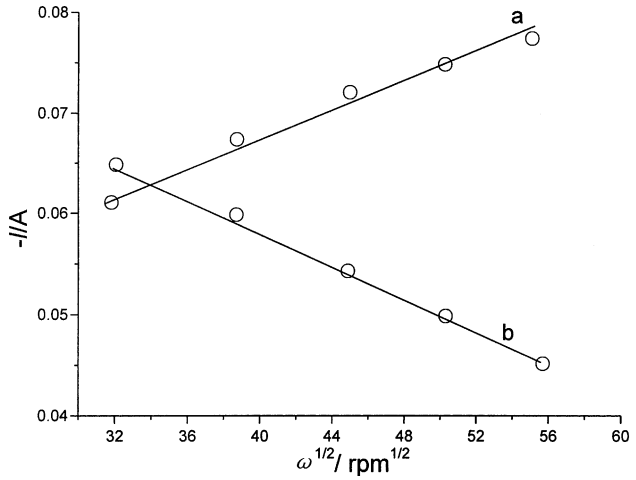

Fig. 4. The plots of I vs. $\omega^{1/2}$ for (a) bath1 and bath2.

SDS acted as a levelling agent, which is also confirmed by the SEM images below.

3.1.4. SEM morphology

Scanning electron microscopy photographs are shown in Fig. 5. Fig. 5(a) and (b) shows the top-view SEM images of alloy1 and alloy2, respectively, and c, d are the magnified images of a and b. The top-view SEM images display the surface morphologies of alloy1 and alloy2. Both shows a homogeneous nodular morphology, which was confirmed by XRD analysis, as shown in Fig. 7(a) and (b). The XRD patterns show that the preferred orientations (1 1 1) for Ni and (0 0 6) for Mg_2Ni in alloy1 and alloy2. The magnified image surface of alloy1, as shown in Fig. 5(d), was rough and coarse and even a few of cracks appeared. A tentative explanation is that the hydrogen evolution on the cathode electrode typically affects crystallization via absorption of the active molecule at a number of growth sites on the surface of pre-critical nuclei, pre-

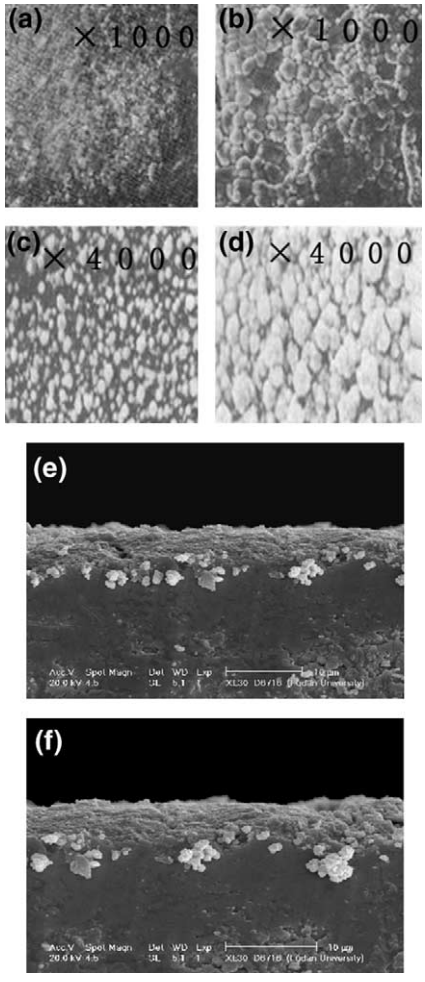

Fig. 5. The images of top-view SEM: (a) alloy1, (b) alloy2, (c) magnification of a, (d) magnification of b and cross-sectional view SEM: (e) alloy1, (f) alloy2.

venting the formation of many alloy nuclei and being beneficial to the growth of nuclei and the formation of a nodular surface [21–23], as was reported by Kelly and Bradley [24] and Bajat and Maskimovic [25]. Owing to the dominance of hydrogen evolution, the Ni–Fe alloy deposit had a coarse surface. Moreover, the dominant hydrogen evolution resulted in the cracks in alloy1, because the reduced hydrogen diffused into the deposit while plating, and was responsible for the internal stress by causing a temporary lattice expansion in the alloy. With the increase in current density, a large amount of hydrogen diffused in the lattice, and the internal stress was greater than the strain energy of the alloy lattice, so that part of the lattices cracked. The release of hydrogen could leave the dendrites or cracks [26,27]. The surface of alloy1, as shown in Fig. 5(a) and (c) was smooth, which confirmed the previous levelling analysis of SDS, because SDS could lower the rate of Mg–Ni alloy deposition, which might allow the deposit to be evenly distributed on the electrode. The morphology showed nodular evenly distributed dark dots surrounded with light rings. The energy spectrum analysis of the SEM showed that the dark dots were Mg (at.17%) and the light rings were almost pure Ni. Thus, there appeared to be a homogeneous arrangement of the surface. The nodular shapes were smaller in alloy2 than in alloy1, which was confirmed by the XRD patterns qualitatively, as shown in Fig. 7. As the 2θ of alloy2 increased, the crystal became smaller.

The cross-sectional SEM micrographs of alloy1 and alloy2 are shown in e and f, respectively, in Fig. 5. Both appear to be textured structures with pores and dendrites. The dendrites might be attributed to the hydrogen and impurities of N, C and S. These impurities were confirmed by EDX analysis, as shown in Fig. 6(a) and (b). The thicknesses of alloy1 and alloy2 were about 4 μm, but EDX analysis as shown in Fig. 6(a) and (b) in the pre-sputter section, containing N, C and S, showed that many organic additives were reduced in the deposition. During 16 min of sputter time, the Ni at.% of alloy1 was higher than that of alloy2, and the Mg at.% of alloy2 was greater than that of alloy1, which was in agreement with the XRD patterns in Fig. 7(a) and (b) and was ascribed to the deposition of SDS complexes with two metal ions, as in Fig. 1.

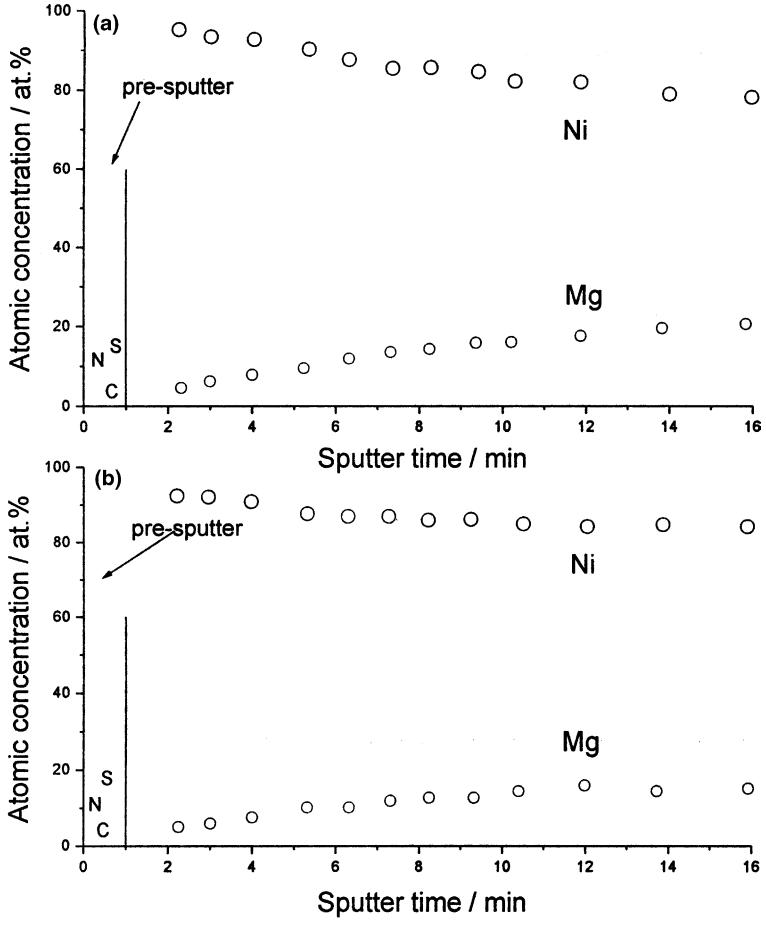

Fig. 6. The results of EDX of (a) alloy1 and (b) alloy2.

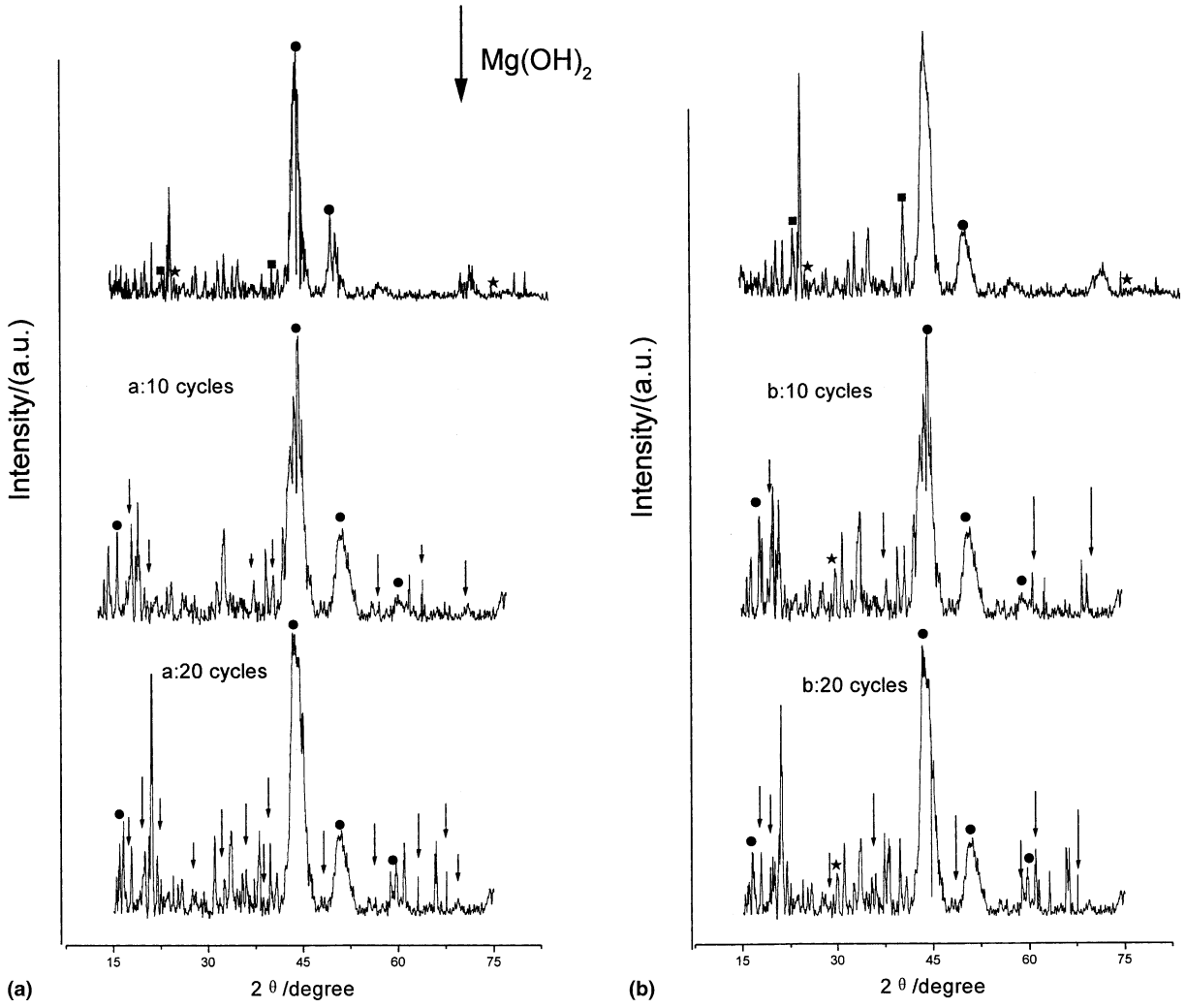

Fig. 7. The XRD patterns for (a) alloy1 and (b) alloy2.

3.1.5. XRD patterns

The XRD patterns of alloy1 and alloy2 are shown in Fig. 7(a) and (b). Two broad and strong peaks were observed in the range of 41–47° (2θ) and in the range of 49° to 54° (2θ), which corresponded to the overlaps of the preferred face-centered cubic (fcc) orientation of Ni (1 1 1) and the preferred body-centered cubic (bcc) orientation of the copper (1 1 1) substrate and the overlaps of fcc (1 1 2) of Ni and bcc (2 0 0) of the copper substrate. The peaks of hexagonal phase Mg_2Ni, were oriented as (0 0 3) at $2\theta = 21°$, (0 0 6) at $2\theta = 40°$; the characteristics peak indexes of Mg_2Ni were in agreement with the reports of a nanometer sized Mg_2Ni–Ni system [28–30]. An interesting result was that the Mg_2Ni peak for alloy2 was stronger than that of alloy1. A tentative explanation could be that SDS is beneficial to the deposition of Mg_2Ni, as in the analysis in Fig. 1. The peaks of Laves phase $MgNi_2$, which appeared as (0 0 4) at $2\theta = 23°$ and (2 2 0) at $2\theta = 79°$, were also in agreement with the reported index of Laves $MgNi_2$[31,32]. A surprising result was that the peaks of hexagonal-close packed (hcp) Mg (0 0 2) at $2\theta = 35°$, (1 0 3) at $2\theta = 63°$ [31] did not appear, which showed that metallic Mg could not exist, Mg was present only in the form of the inter-metallic Mg–Ni alloy.

At $2\theta = 30°$, the peak of $C_{12}H_{12}N_2$ appeared and IR, MS and ^1H NMR measurements were carried out in order to understand its composition. The spectra are shown in Fig. 8(a)–(c) respectively. According to the formula of the unknown compound, the number of unsaturated carbon atoms is 11. At 3243 cm^{-1}, a strong IR peak appeared, it is characteristics of ν_{N-H}. At 1680, 1575, 1563 and 1471 cm^{-1}, four strong absorption peaks appeared characteristic of benzene stretch vibrations [33]. In MS, the values of m/z of 77, 66, 51 and 42, indicated the stripping peaks of benzene and 137, 122 and 165 indicated the stripping peaks of pyrazine [33]. In ^1H NMR, peaks at $\delta = 6.5$–8.5 and $\delta = 2.5$ indicated Ph–H and N–H, respectively; the height of the former was 4, the height of the latter was 1. Therefore, the unknown compound was phenothiazine [33].

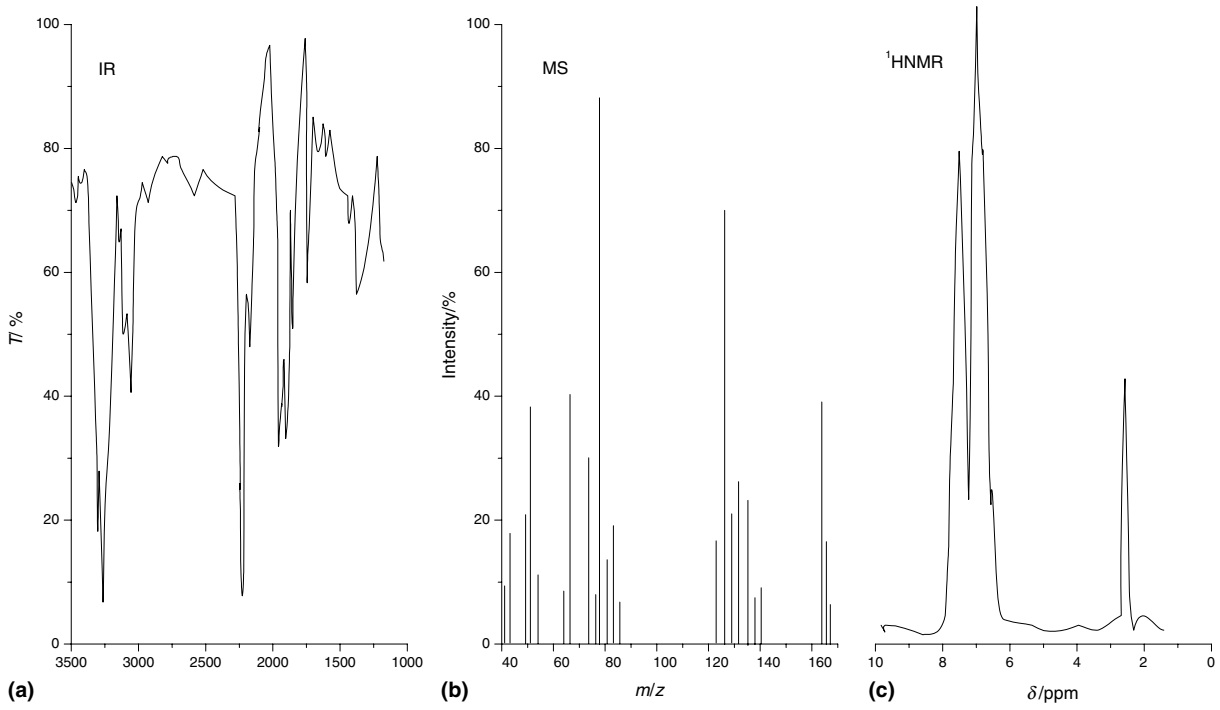

Fig. 8. The (a) IR, (b) MS and (c) ^{1}H NMR of the unknown compound.

3.2. The influence of SDS on the hydrogen absorption of Mg–Ni alloy

3.2.1. P–C isotherms

The P–C isotherms for alloy1 and alloy2 are shown in Fig. 9; the value H/M of both alloy1 and alloy2 was 0.9, which was close to the ratio H/M = 1.02 of a nanometer Mg_2Ni–Ni composite obtained by mechanical alloying [34], and lower than that found for Mg_2Ni, 1.2 [35]. The plateau of alloy2 was higher than that of alloy1, which showed that the capacity for hydrogen absorption of alloy2 was greater than that for alloy1, for three possible reasons: first, the Mg–Ni alloy could absorb hydrogen due to the presence of Mg_2Ni, as Mg_2Ni is known to be a good hydrogen absorption material [36–38]. The analysis of the XRD patterns and EDX showed that alloy2 contained more of the Mg_2Ni phase than alloy1. Second, the evenly distributed phenothiazine codeposited with alloy2 possessed an outer layer of electron donor–acceptor (EDA) species, which was probably involved in activating the hydrogen atom and then transferred to the adjoining sites of Mg_2Ni by a diffusion spillover process [39]; from the Hückel $4n+2$ Rule [40] that aromatic compounds have 2, 4, 6$\cdots$Π-electrons, the composition of phenothiazine is as follows:

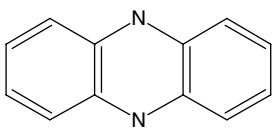

This has 10 Π-electrons, so it is evident that the cyclic Π-electron system would be beneficial in activating alloy2 in the course of hydrogen absorption. Third, alloy2 has more dendrites, and it is reasonable that a hydrogen storage materials with dendrites is better able to absorb hydrogen [41–44].

As shown in Fig. 9, there is only one plateau in alloy1 and alloy2; this also showed that the Mg phase did not appear in the Mg–Ni alloy deposit, or else, two plateaus would be observed in alloy1 and alloy2, as in the imaginary curve c shown in Fig. 9, as was reported by

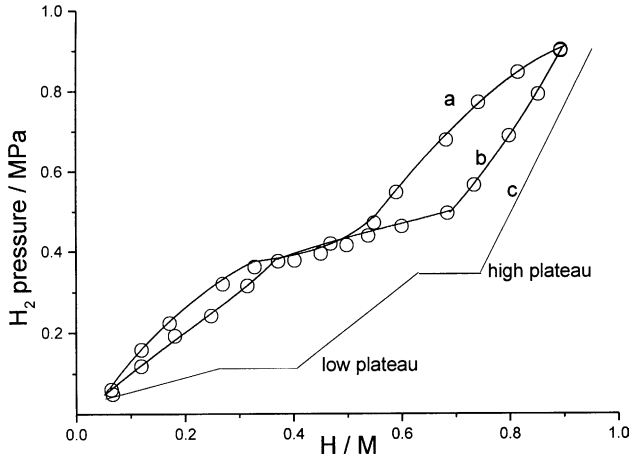

Fig. 9. Hydrogen absorption isotherms for (a) alloy1, (b) alloy2 and (c) imaginary Mg+Mg_2Ni alloy.

Sun and Gingl [45], who found a lower pressure for Mg hydride,

$$Mg + H_2 \rightarrow MgH_2$$

and a higher pressure for Mg_2Ni hydride,

$$Mg_2Ni + H_2 \rightarrow Mg_2NiH_4.$$

This is also in agreement with the result of XRD above.

3.2.2. Discharge capacity of the alloy

Fig. 10 shows the relation of discharge capacity and cycle number within 20 charge–discharge cycles for alloy1 and alloy2. It is noted that the maximum discharge capacities of alloy2 and alloy1 were 388 and 203 mA h/g, respectively, which is in line with the results of PCT. It was reported that the discharge capacity of Mg_2Ni, obtained by mechanical alloying, was 250 mA h/g [35]. Compared to alloy2, the discharge capacity of alloy1 decayed markedly with increasing cycle number. As shown in Fig. 7(a) and (b), there were more $Mg(OH)_2$ peaks after 20 cycles than after 10 cycles for both alloy1 and alloy2. Evidently, there were more $Mg(OH)_2$ peaks within the same cycles for alloy1 than that of alloy2.

From Fig. 7(a) and (b) it could be seen that the $Mg(OH)_2$ phase occurred after 10 and 20 cycles of charging/discharging, suggesting that Mg from the Mg_2Ni phase (which was discussed elsewhere [46]) on the alloy surface was oxidized to $Mg(OH)_2$ during charge–discharge cycles in alkaline solution, simultaneously leading to the appearance of Ni peaks in XRD patterns of alloy surface. The related reaction equation is :

$$Mg_2Ni + 4OH^- \rightarrow 2Mg(OH)_2 + Ni + 4e^-$$

This indicates that decay of the discharge capacity of alloy1 and alloy2 with increasing cycle number was mainly due to the formation of $Mg(OH)_2$ on the alloy surface, because Mg_2Ni had the characteristics of hydrogen storage, due to the hydrogen storage function of Mg [39]. The oxidation of Mg had to decrease the hydrogen capacity for each discharge cycle. In addition, the $Mg(OH)_2$ layer on the alloy surface might lower the alloy electrochemical reactivity and work as a barrier preventing diffusion of hydrogen into or from the alloy bulk. Mg_2Ni alloy from mechanical grinding had similar decay properties, reported by Iwakura et al. [47].

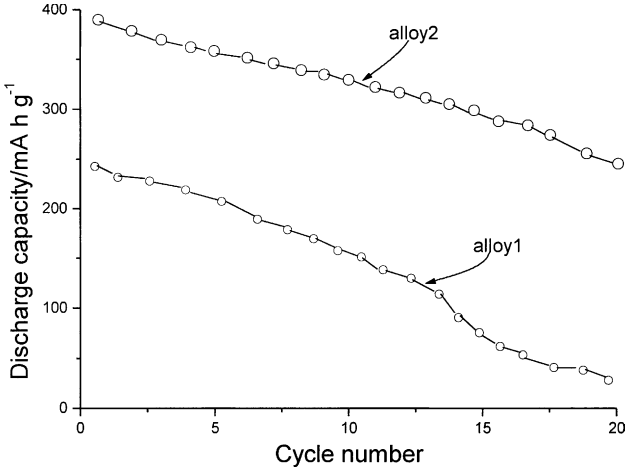

Fig. 10. Discharge capacity as a function of cycle number for alloy1 and alloy2.

3.2.3. Electrochemical impedance spectroscopy

According to the theory of Rubinstein [48], electrochemical impedance spectroscopy has been regarded as a very practicable tool for studying electrode materials and batteries. The measurement results could reveal information about the molecular kinetics of reactions for electrode materials in a battery during charge/discharge courses. The impedance spectra of batteries of alloy1 and alloy2 were used in the equivalent circuit as shown in Fig. 11(a), where R_1 of the solution resistance is used to account for the resistance of ions through KOH aqueous solution. R_2 and C_2 correspond to the contact resistance and contact capacity between Mg–Ni alloy and the copper electrode, respectively. R_{ct} is the charge transfer resistance across the Mg–Ni alloy|electrolyte interface. Z_w is the diffusion impedance in the Mg–Ni alloy, and this was believed to be due to the diffusion of hydrogen in the Mg–Ni alloy. The expected Nyquist plot of the above proposed circuit is presented in Fig. 11(b). Part (i) is due to the solution resistance R_1, the small arc (ii) is due to contact resistance R_2, the large arc (iii) is due to reaction resistance R_{ct}, the linear part (iv) is due to diffusion impedance Z_w. EIS measurements of the test battery after 10 and 20 charge/

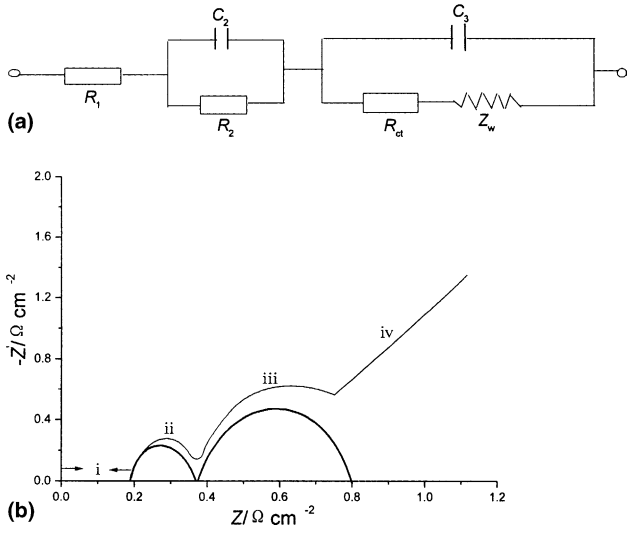

Fig. 11. (a) An equivalent circuit to represent the impedance of the test battery using a Mg–Ni alloy positive electrode and (b) the expected Nyquist plot for (a).

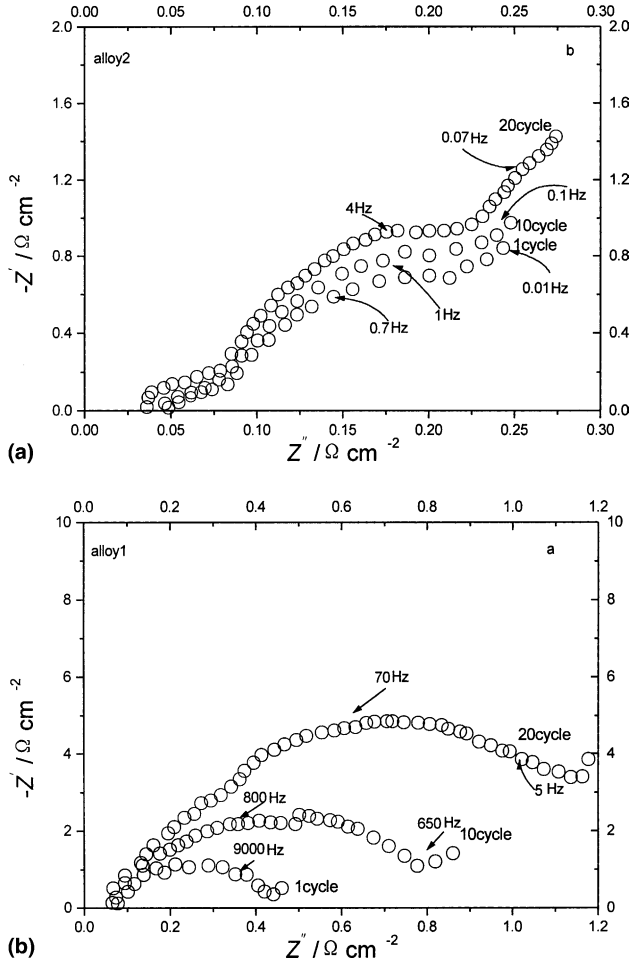

Fig. 12. The impedance spectra of alloy1 (a) and alloy2 (b) after charge–discharge cycles.

discharge cycles for alloy1 and alloy2 were performed at different potentials. As shown in Fig. 12(a) and (b), with increasing charge/discharge cycle number, the reaction resistance and diffusion impedance of alloy1 and alloy2 both increased and the blocking force of the absorption/desorption of hydrogen was enhanced; in other words, it was disadvantageous to the charge/discharge cycling of the Mg–Ni alloy. Compared to alloy1, both the reaction resistance and diffusion impedance of alloy2 increased less markedly; this indicated that alloy2 was more favorable for the electrochemical hydriding reaction.

4. Conclusion

In the Mg–Ni alloy electrodeposition process, owing to the absorption of SDS on the cathode electrode, SDS could inhibit the hydrogen evolution and lower the alloy deposition rate. The analysis of RDE measurements showed SDS had a levelling effect in the Mg–Ni alloy deposition, which resulted in a smooth surface of the Mg–Ni alloy; the ratio H/M of alloy2 was 0.9. The first discharge capacity of alloy2 was 388 mA h/g.

Acknowledgements

The authors wish to thank Prof. Cheng for SEM and EDX work, Prof. Li for spectral work and acknowledge the support of the Shanghai Educational Committee, China, and of the Shanghai Educational Development Foundation, China (99SG39), through the Knowledge Innovation Projects, Chinese Academy of Sciences (kzcxz-409).

References

[1] S. Orimo, H. Fujii, J. Alloys Comp. 232 (1996) L16.
[2] T. Spassov, U. Koster, J. Alloys Comp. 287 (1999) 243.
[3] T. Kohno, M. Kanda, J. Electrochem. Soc. 144 (1997) 2384.
[4] T.C. Franklin, T.S. Sankara-Naryanan, J. Electrochem. Soc. 143 (1996) 97.
[5] T.C. Franklin, M. Ohta, Surf. Technol. 18 (1982) 63.
[6] T.C. Franklin, V. Totten, S. Jackson, G. Jacobs, Surf. Technol. 81 (1994) 48.
[7] T.C. Franklin, J. Chappel, R. Fierro, A.I. Aletan, R. Wicknan, Surf. Coat Technol. 34 (1988) 515.
[8] T.C. Franklin, J. Darlington, S.L. Cooke Jr., J. Electrochem. Soc. 107 (1960) 556.
[9] T.C. Franklin, J. Darlington, J. Electrochem. Soc. 133 (1986) 893.
[10] T.C. Franklin, R. Sothern, J. Phys. Chem. 58 (1954) 951.
[11] A. Montaser, V.A. Fassel, Anal. Chem. 48 (1976) 1490.
[12] L.G. Sillen, A.E. Martell, Stability Constants: Metal–ion Complexes, second ed., Academic Press, London, 1964.
[13] T.M. Harris, G.M. Whitely, J. Electrochem. Soc. 142 (1995) 1031.
[14] J. Wang, Stripping Analysis Principles, Instrumentation and Applications, VCH, Weinheim, 1985.
[15] S. Trastatti, J. Electrochem. Soc. 13 (1979) 81.
[16] R.M. Reeves, Modern Aspects of Electrochemistry, Plenum Press, New York, 1974.
[17] F. Yang, S.M. Zhou, Xiamen Univ. Acta 13 (1989) 220.
[18] G.T. Royers, K.T. Taylor, Metal Finish. 43 (1965) 75.
[19] O. Kardos, Plating 61 (1974) 129.
[20] S.S. Kruylikly, N.T. Kudryavtsey, R.P. Soboley, Electrochim. Acta 12 (1967) 1263.
[21] R. Albalat, E. Gomez, C. Muller, J. Appl. Electrochem. 21 (1991) 109.
[22] E. Gomez, E. Valles, J. Electrochem. Soc. 495 (2000) A19.
[23] C. Karwas, T. Hepel, J. Electrochem. Soc. 135 (1998) B839.
[24] J.J. Kelly, P.E. Bradley, J. Electrochem. Soc. 147 (2000) 2975.
[25] J.B. Bajat, M.D. Maskimovic, J. Appl. Electrochem. 31 (2001) 355.
[26] E.V. Potter, R.W. Huber, Phys. Rev. 68 (1945) 24.
[27] J. Gong, G. Zangari, J. Electrochem. Soc. 149 (2002) C209.
[28] H. Fujii, S. Orimo, K.I. Keda, J. Alloy Comp. 253 (1997) 80.
[29] K. Tanaka, H. Tanaka, H. Tanaka, J. Alloy Comp. 256 (2002) 330.
[30] T. Kohno, S. Tsuruta, M. Kanda, J. Electrochem. Soc. 143 (1996) L198.
[31] H. Kakuta, A. Kamrgawa, H. Takamura, Mater. Sci. Forum 350 (2000) 329.
[32] P. Villars, L.D. Calvert, Pearson's Handbook of Crystallographic Data for Intermetallic Phases, 2nd ed., ASM International, Materials Park, OH, 1991.

[33] D.H. Willians, Spectroscopic Methods in Organic Chemistry, third ed., McGraw-Hill, London, 1980.
[34] C. Iwakara, H. Inoue, J. Alloys Comp. 270 (1998) 142.
[35] T. Kohno, M. Kanda, J. Electrochem. Soc. 144 (1997) 2384.
[36] R.J. Reilly, R.H. Wiswell, Inorg. Chem. 7 (1968) 2254.
[37] L. Sun, P. Yan, J. Alloys Comp. 293 (1999) 536.
[38] T. Kohno, M. Manda, J. Electrochem. Soc. 44 (1997) 2343.
[39] P. Selvanm, B. Viswanathan, C.S. Swamy, J. Int. Hydrogen Energy 11 (1986) 1692.
[40] G. Marc London, Organic Chemistry, Addison Wesley, Reading, MS, 1984, p. 568.
[41] T. Mutschde, R. Kircheim, Sur. Metall. 21 (1987) 1101.
[42] M. Hirscher, S. Zimmer, H. Kronmuller, J. Phys. Chem. 183 (1994) 51.
[43] S.M. Tadyyon, O. Yoshinari, J. Appl. Phys. 32 (1993) 3928.
[44] K. Tanaka, M. Otsuka, Int. J. Hydrogen Energy 24 (1979) 891.
[45] D. Sun, F. Gingl, Mater. Acta 48 (2000) 2363.
[46] I. Galus, Fundaments of Electrochemical Analysis, Ellis Horwood, New York, 1976, p. 247.
[47] C. Iwakura, R. Shin-ya, K. Miyanohara, S. Nohara, H. Inoue, Electrochim. Acta 46 (2001) 2781.
[48] I. Rubinstein (Ed.), Physical Electrochemistry, Marcel Dekker, New York, 1978.